Turkish Journal of Engineering

Turkish Journal of Engineering (TUJE)
Vol. 2, Issue 2, pp. 54-59, May 2018
ISSN 2587-1366, Turkey
DOI: 10.31127/tuje.349532
Research Article

EXPERIMENTAL INVESTIGATION OF FLOW STRUCTURE DOWNSTREAM OF PERMEABLE CYLINDERS

Bengi Gözmen Şanlı *[1] and Hüseyin Akıllı [2]

[1] Mersin University, Faculty of Engineering, Department of Mechanical Engineering, Mersin, Turkey
ORCID ID 0000 – 0001 – 6805 – 2454
bengigozmen@mersin.edu.tr

[2] Cukurova University, Faculty of Engineering & Architecture, Department of Mechanical Engineering, Adana, Turkey
ORCID ID 0000 – 0002 – 5342 –7046
hakilli@cu.edu.tr

* Corresponding Author
Received: 06/11/2017 Accepted: 07/12/2017

ABSTRACT
Flow structure downstream of permeable cylinders was investigated using high-image density Particle Image Velocimetry technique in deep water. The free stream velocity is U_∞= 156 mm/s, which corresponds to the Reynolds number of Re=6250 based on the cylinder diameter D=37.5 mm. To reveal the effect of the porosity, four different porosities (β= 0.4, 0.5, 0.6 and 0.7) were used. This study showed that the usage of permeable cylinder decreases the occurrence of large-scale vortical structures downstream of the bluff body. As the porosity increases, turbulent kinetic energy, Reynolds shear stress and intensity of turbulences decrease as a sign of attenuated fluctuations in the wake region. For the permeable cylinders having the porosity higher than 0.6, the flow behaves as there is no object in flow.

Keywords: *PIV, Vortex Shedding, Permeable Cylinder, Deep Water*

1. INTRODUCTION

Circular cylinder is one of the most commonly used structures in many engineering applications because of its geometrical simplicity. In despite of the simple geometry, the flow around the cylinder is enough to explain complex phenomenon in the wake region. Therefore, many researchers have focused on the circular cylinder at the last century. Control of vortex shedding downstream of circular cylinders has a great importance and several control methods are used to suppress the pattern effect of vortex shedding. These methods are active and passive controls. At active control methods, there is an energy input into the flow region while passive control methods are based on the geometrical adjustments. Plasma actuators (Corke *et al*., 2010), synthetic jets (Feng and Wang, 2012; Akansu and Fırat, 2010), feedback controls (Muddada and patnaik, 2010; Hiejima *et al*., 2005) and suction and blowing (Li et al., 2003) are some of the active control methods. On the other hand, many passive control methods are used at the studies since applying passive control methods are easier than that of the active control methods. Gim *et al.* (2011) used control rods to control the flow. They attached the rod to the rearward stagnation point of a circular cylinder. They investigated the effect of sizes of control rods and Reynolds number. Lim and Lee (2003) researched the flow structure around a circular cylinder with U-grooved surfaces. They presented that the U-shaped grooves reduce the drag coefficient by18.6%, compared with that of plain cylinder. The Longitudinal grooves shifted the vortices position and shortened the vortex formation region in comparison to the plain cylinder. Nakamura and Igarshi (2008) controlled the vortex shedding by attaching cylindrical rings around the cylinder. They reduced drag and fluctuating forces. The drag force decreased by 15% for $Re_d \geq 20\ 000$. Ekmekci and Rockwell (2010) investigated experimentally the effect of a single wire attached on the outer surface and parallel to span of a stationary circular cylinder and they defined two critical angles effective on near-wake structure. At one critical angle, substantial extension occurred and at the other critical angle, significant contraction of the time-averaged near-wake bubble was obtained. Sahin and Smith (1987) used two perforated plates in order to control the velocity distribution emerging from a wide-angle, three-dimensional diffuser of area ratio 6.8. They showed that the most uniform velocity distributions in the collection chamber downstream of the diffuser were provided using two perforated plates of porosity $\beta = 0.5$. The best results were obtained with one of the plates positioned a short distance downstream of the diffuser entry plane ($L/W = 0.14$) with the second plate just upstream of the exit plane ($L/W=0.79$). Farhadi *et al.* (2010) studied on two-dimensional unsteady laminar flow over a semi-circular cylinder near a splitter plate numerically. They carried out numerical simulations for different Reynolds numbers ranging from 100 to 500 in three different gaps ($g = 0.0D$ to $4.5D$) and two different splitter lengths ($LSP = 1$ and $2D$). Their results of study signified that the vortex shedding formed in the wake and the oscillating amplitude of the lift coefficient was decreased by increasing the gap ratio. Sudhakar and Vengadesan (2012) researched the vortex shedding characteristics of a circular cylinder attached with an oscillating splitter plate, numerically. They forced the splitter plate to exhibit the simple harmonic motion. Gozmen *et al.* (2013) investigated the effect of splitter plates having different heights and lengths located in the wake region of the circular cylinder in shallow water. The results of their study pointed out that flow structures changed significantly with height and length ratios of the splitter plates in shallow water. The wake region downstream of the cylinder lengthened along the streamwise direction with increasing the plate length and depth. Al-Hajeri *et al.* (2009) investigated two-dimensional laminar flow past three circular porous cylinders arranged in an in-line array numerically. For the same range of Reynolds number (312-520), they indicated that flow behavior around the solid cylinder differed from the flow around the porous cylinders. The flow characteristics around solid cylinders were determined by the Reynolds number, whereas the flow characteristics around the porous cylinders were determined by the V (i)/V (f) ratio. Ozkan *et al.* (2012) carried out a study on the flow control around a circular cylinder surrounded by a permeable cylinder in shallow water. They revealed that both the porosity value and the diameter ratios were significant parameters on the suppression of vortex shedding downstream of the circular cylinder. Pinar *et al.* (2015) performed a study on the control of flow around the perforated cylinders having the porosities in the range of $0.1 \leq \beta \leq 0.8$ with an increment of 0.1. They presented that the fluctuations were reduced dramatically in the wake region by the use of perforated cylinders having the porosities in the interval of $0.4 \leq \beta \leq 0.8$. To reveal the effects of porosity on the suppression of vortex shedding, Gozmen and Akilli (2014) used permeable cylinders having various porosities and diameters to control the flow downstream of a solid cylinder. They indicated that the outer permeable cylinder decreased the wake instabilities and vortex shedding downstream of the cylinder arrangement depending on the porosity and the diameter ratio in deep water.

The main aim of this study is to investigate the flow structure downstream of the permeable cylinders having different porosities in deep water. In order to use permeable cylinders instead of solid cylinders, the vortex shedding in the wake region of only permeable cylinder was investigated inclusively. The experiments were conducted using permeable cylinders having four different porosities β with the diameter of cylinder $D=37.5$ mm.

2. EXPERIMENTAL SETUP

Experiments were carried out in a circulating rectangular open channel located at Fluid mechanics laboratory of mechanical engineering department of Çukurova University. The test section has a length of 8000 mm, a width of 1000 mm and a height of 750 mm. The PIV technique was applied to calculate the instantaneous and time-averaged velocity vector fields downstream of permeable cylinders. The free stream velocity, U was fixed at 156 mm/s as the Reynolds number was about 6250 depending on the diameter of permeable cylinder. The side view of experimental system is presented in Figure 1. Four different porosity values (β= 0.4, 0.5, 0.6, and 0.7) were selected to pointed out the effect of permeable cylinder having

different porosity on the flow structure. Meanwhile, porosity is defined as the ratio of gap area on the body to the whole body surface area. All permeable cylinders are made of a chrome-nickel wire mesh. During the experiments, the total depth of the water in the channel was adjusted 560 mm while the water height was maintained at 340 mm which corresponded to the distance from free surface to the base of the platform. The measurement of flow field was made at the mid-depth (h_L) of water above the platform. The permeable cylinder was placed to the location which was 1750 mm far away from the leading edge of the platform to assure the fully-developed boundary layer. The geometric blockage ratio was 4.5 %.

The experimental measurements were performed by using a PIV system. The PIV system is consisting of a pair of doubled-pulsed Nd:YAG laser, a CCD camera, a synchronizer and a grabber. A pair of double-pulsed Nd:YAG laser light sheet lightened the flow. The thickness of laser sheet was about 2 mm and the laser sheet was parallel to the surface of the platform during all experiments. As seeding particles, silver-coated hollow glass spheres with a mean diameter of 12 µm and a density of 1100 kg/m^3 were chosen which were assumed to follow the flow dynamics accurately. In addition, the non-dimensional Stokes number was calculated as 1.83×10^{-4} (Raffel *et al.*, 1998) for these particles. During the experiments, the images were recorded using a 8-bit charged-coupled device (CCD) camera with a resolution of 1600x1200 pixels, equipped with a Nixon AF micro 60 f/2.8D lens and furthermore, the camera and laser pulses were synchronized by a synchronizer.

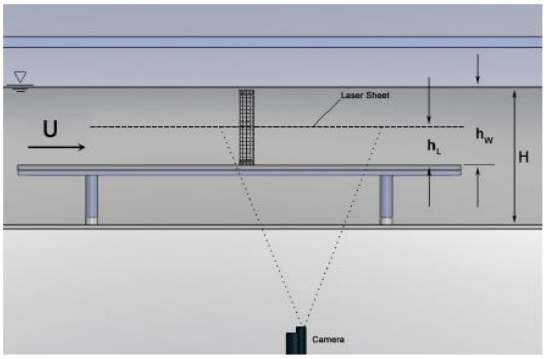

Fig. 1. Side view of experimental system

Quantative flow images were processed by Flow Manager Software. The cross-correlation method based on the Fast-Fourier-Transform (FFT) was used to calculate particle displacement. The interrogation area was selected as a grid size of 32x32 pixels overlapping by 50 %, which resulted in a set of 3844 vectors (62x62) for the flow field. In each experiment, 350 instantaneous images were captured and stored to calculate averaged-velocity vectors and other statistical properties of the flow field. During the experiments, two views one after the other were taken and every field of view was taken as 200x200 mm^2. The total uncertainty in velocity relative to depth-averaged velocity was estimated to be about 2 % for this arrangement.

3. RESULTS AND DISCUSSION

Fig. 2 displayed the Reynolds shear stress contours of permeable cylinders having the diameters of D=37.5 mm. To illustrate the effect of porosity, the Reynolds shear stress contours of bare cylinder and permeable cylinders having four different porosity values (β = 0.4, 0.5, 0.6 and 0.7) are shown in this figure. At this figure, the minimum and incremental values of $< u'v' >$ were taken as 0.0015 and 0.0015, respectively. The solid lines demonstrate positive (counter-clockwise) contours of Reynolds shear stress while the dashed lines demonstrate the negative (clockwise) contours. The normalized Reynolds shear stress contours determine significant information about the fluctuations in the wake region. It is clearly understood that the peak magnitude of Reynolds shear stress of the bare cylinder is about 0.048 and both large-scale clusters caused by the unsteady vortex shedding and small-scale clusters due to the small-magnitudes of the oscillations in the near wake of the cylinder are seen downstream of the bare cylinder. For the porosities of β = 0.4, 0.5, 0.6 and 0.7, in contrast to the bare cylinder case, there is no a distinct concentration in the Reynolds shear stress contours. The peak values o

f $< u'v' >$ are several times smaller than that of the bare cylinder case. As the porosity values increase, the concentration of Reynolds shear stress decreases significantly and the location of peak concentration of Reynolds shear stress moves further away from the base of the cylinder as a result of the increase in the open area on the surface of the permeable cylinder. For the porosities of β = 0.4, the peak magnitude of Reynolds shear stress is determined to be 0.0209. With increasing the porosity values from 0.6 to 0.7, the concentration of Reynolds shear stress significantly weakens at the centerline of the permeable cylinder. This decrease in the Reynolds shear stress may be directly related to the drag force reduction at the flow region as obtained by Fujisawa and Takeda (2003).

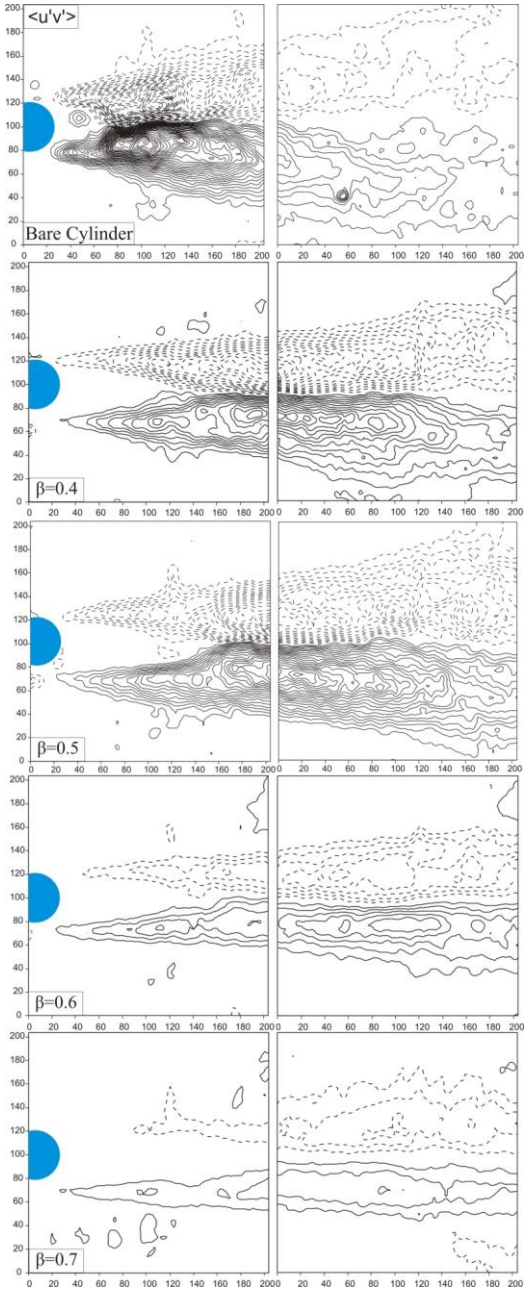

Fig. 2. Contours of Reynolds shear stress for the diameter of 37.5 mm

The time-averaged streamline topologies for various porosities at the cylinder diameters of D=37.5 mm are illustrated in Fig. 3. For bare cylinder case, two focus points (F1, F2) emerge in the close region of cylinder and a saddle point S occurs at the location which is considered at the end of vortex formation. Two-well defined foci, F1, F2 are nearly symmetrical with regard to the centerline and the shear layers occur in the first field of view. When all permeable cylinder cases are examined, the streamline topologies represent that neither foci nor saddle point appear downstream of the cylinder due to reduction in transverse velocity in the wake region. The streamlines lengthen in the streamwise direction without any circulation. Due to the non-appearance of the focal flow structure downstream of the permeable cylinder, the wake region length cannot be designated.

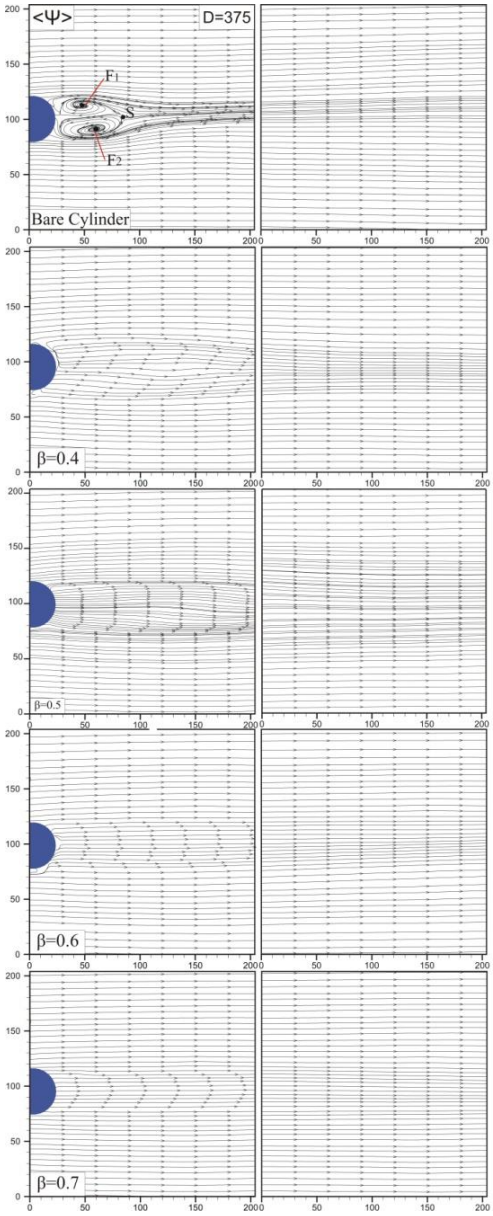

Fig. 3. Patterns of time-averaged streamline topologies for permeable cylinder having the diameter of 37.5 mm

The relationship between the peak value of turbulent kinetic energy and the porosity for the permeable cylinder and the peak value of turbulent kinetic energy of bare cylinder are indicated in Fig. 4 to reveal the effect of the porosity on the flow characteristics. The peak value of TKE of bare cylinder is greater than those of all permeable cylinders as a sign of large scale vortices which transfer momentum from the free-stream flow into the wake region. For permeable cylinders, the peak value of TKE decreases progressively with increasing of the porosity. For the porosity of $\beta = 0.7$, the peak value of TKE decreases to 0.019 several times smaller than that of the bare cylinder. This is an expected result since the open area on the surface of the permeable cylinder enlarges with the enhancement of

the porosity value. This implies that the permeable cylinders having the porosity higher than 0.6 do not pose an obstacle for the flow. This outcome is in accord with the results of Reynolds shear stress and the time-averaged streamline topologies.

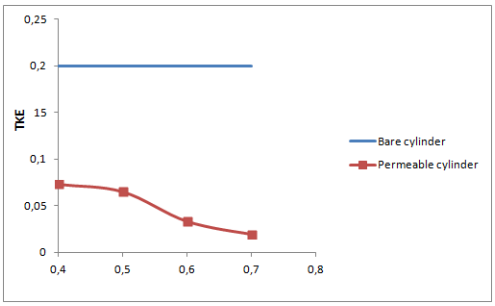

Fig. 4. The variation of peak value of TKE as a function of porosity for the permeable cylinder and peak value of TKE for bare cylinder

Fig. 5 presents contours of the time-averaged streamwise velocity <u>/U for the bare cylinder case and the permeable cylinder cases. The dashed lines present negative values of <u>/U, whereas the solid lines indicate positive values. The minimum and incremental values of the streamwise velocity contours were selected as ± 5 and 5, respectively. The substantial region of reverse flow is seen at the downstream of the bare cylinder as a consequence of the momentum transfer from the free-stream region into the wake region. The peak value of negative streamwise velocity is nearly 0,160. When the effects of permeable cylinders are examined, it is observed that the reverse flow does not form in the fields of view for all porosity values and the minimum value of streamwise velocity component increases and the location of the minimum value of streamwise velocity moves further downstream of the permeable cylinder with increasing the porosity.

The spectra of streamwise velocity fluctuations depicted in Fig. 6 (A) are evaluated at a certain location (A) which is 1D far away from the base of the cylinder for the bare cylinder and permeable cylinders having four different porosity values. For the bare cylinder case, natural frequency of vortex shedding is found to be f=0.73 Hz as a sign of occurrence of vortical structure in the wake region of the bare cylinder. For permeable cylinder cases, any clear and distinct peak of frequency cannot be observed. This denotes that the vortex shedding in the wake region is prevented. This result justifies the other evidences obtained from other figures in this study.

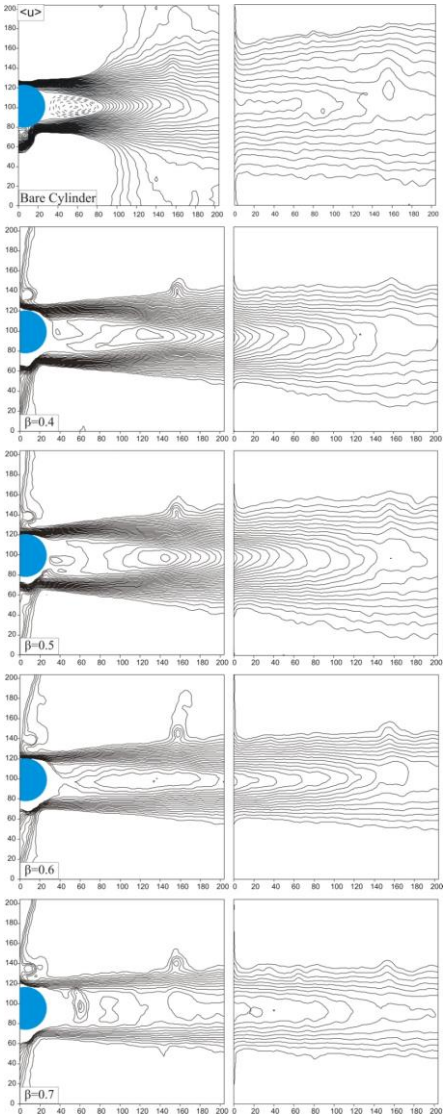

Fig. 5. Contour patterns of time-averaged streamwise velocity <u>/U for bare cylinder and the permeable cylinders having four different porosity values.

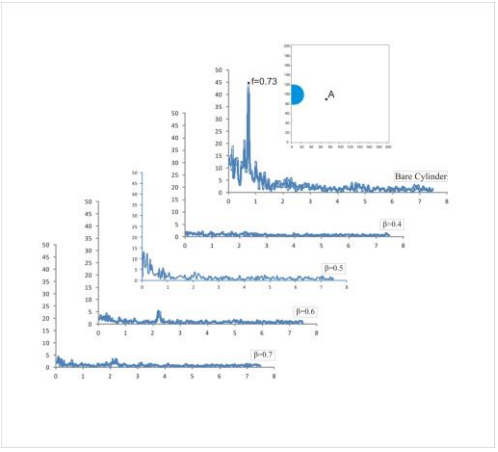

Fig.6. Spectral analysis of bare cylinder and permeable cylinders having the diameter of D=37.5 mm

4. CONCLUSION

In present study, the influence of permeable cylinder on the wake flow is experimentally investigated by the PIV technique in deep water. Four different porosity values for the permeable cylinders having D=37.5mm were used to find out the effects of permeable cylinder. During the experiments, the Reynolds number was about 6250 depending on the diameter of permeable cylinder. In order to explain the effect of the permeable cylinder, the time-averaged streamwise velocity, the time averaged patterns of streamlines and Reynolds shear stress contours are illustrated at this study. A result taken into consideration is that the occurrence of large-scale vortical structures is suppressed by permeable cylinders. The peak values of TKE and Reynolds shear stress decrease gradually with increasing of the porosity. When the results are evaluated in terms of the frequency of vortex shedding, any clear and distinct peak of frequency cannot be obtained at the downstream of the permeable cylinders as the natural frequency of vortex shedding is found to be f=0.73 for the bare cylinder case. The flow structures at the wake region of permeable cylinders having porosity values $\beta \geq 0.6$ are like a flow without an obstacle in the flow field. This means that occurrence of vortex shedding and energy transfer from the free stream region into the wake region are considerably prevented. Thus, the permeable cylinders having the porosities $\beta \geq 0.6$ would be used instead of the solid cylinders at the many engineering applications.

REFERENCES

Akansu, Y. E. and Fırat, E. (2010). "Control of flow around a square prism by slot jet injection from the rear surface." *Experimental Thermal and Fluid Science*, Vol. 34, No. 7, pp. 906-914.

Al-hajerı, M. H., Aroussi, A. and Witry, A. (2009). Numerical Simulation of Flow Past Multiple Porous Cylinders. *Journal of fluids engineering-transactions of the ASME*, Vol. 131, No. 7, 071101.

Corke, T. C., Enloe, C. L. and Wilkinson, S. P. (2010). Dielectric barrier discharge plasma actuators for flow control. Annual Review of Fluid Mechanics, Vol. 42, pp. 505-529.

Ekmekci, A and Rockwell, D. (2010). Effects of a geometrical surface disturbance on flow past a circular cylinder: a large-scale spanwise wire. *Journal of Fluid Mechanics*, Vol. 665, pp. 120-157.

Farhadi, M, Sedighi, K and Fattahi, E. (2010). Effect of a splitter plate on flow over a semi-circular cylinder. Proc. IMechE Part G: *J. Aerospace Engineering*, Vol. 224, pp. 321-330.

Feng, L-H and Wang, J. J. (2012). Synthetic jet control of separation in the flow over a circular cylinder. *Experiments in Fluids*, Vol. 53, pp. 467–480.

Fujısawa, N. and Takeda G. (2003). Flow Control Around a Circular Cylinder by Internal Acoustic Excitation. *Journal of Fluids and Structures*, Vol. 17, pp. 903– 913.

Gim, O. S., Kim, S. H. and Lee, G. W. (2011). Flow control behind a circular cylinder by control rods in uniform stream. *Ocean Engineering*, Vol. 38, No. 17-18, pp. 2171–2184.

Gozmen, B., Akilli, H. and Sahin, B. (2013). Passive control of circular cylinder wake in shallow flow. *Measurement*, Vol. 46, pp. 1125-1136.

Gozmen, B. and Akilli, H. (2014). Flow control downstream of a circular cylinder by a permeable cylinder in deep water. *Wind and Structures*, Vol. 19, No.4, pp. 389-404.

Hiejima, S., Kumao, T. and Taniguchi, T. (2005). Feedback control of vortex shedding around a bluff body by velocity excitation. *International Journal of Computational Fluid Dynamics*, Vol. 19, No. 1, pp. 87-92.

Li, Z., Navon, I. M., Hussaini, M. Y. and Le Dimet, F-X. (2003). Optimal control of cylinder wakes via suction and blowing. *Computers & Fluids*, Vol. 32, pp. 149–171.

Lim, H. C and Lee, S. J. (2003). PIV Measurements of near wake behind a U-grooved cylinder. *Journal of Fluids and Structures*, Vol. 18, No. 1, pp. 119-130.

Muddada, S. and Patnaik, B. S. V. (2010). An assessment of turbulence models for the prediction of flow past a circular cylinder with momentum injection. *Journal of Wind Engineering and Industrial Aerodynamics*, Vol. 98, pp. 575-591.

Nakamura, H and Igarshi, T. (2008). Omnidirectional reductions in drag and fluctuating forces for a circular cylinder by attaching rings. *Journal of Wind Engineering and Industrial Aerodynamics*, Vol. 96, pp. 887–899.

Ozkan, G. M., Oruc, V., Akilli, H. and Sahin, B. (2012). Flow around a cylinder surrounded by a permeable cylinder in shallow water. *Experiments in Fluids*, Vol. 53, No. 6, pp. 1751-1763.

Pinar, E., Ozkan, G. M., Durhasan, T., Aksoy, M. M., Akilli, H. and Sahin, B. (2015). Flow structure around perforated cylinders in shallow water. *Journal of Fluids and Structures*, Vol. 5, pp. 52–63.

Raffel, M., Willert, C. E. and Kompenhans, J. (1998) Particle Image Velocimetry a Practical Guide, Springer, Göttingen.

Sahın, B. and Ward-Smith A. J. (1987) The use of perforated plates to control the flow emerging from a wide-angle diffuser. *Heat and Fluid Flow*, Vol. 8, No. 2, pp. 124-131.

Sudhakar, Y. and Vengadesan, S. (2012). Vortex shedding characteristics of a circular cylinder with an oscillating wake splitter plate. *Computers & Fluids*, Vol. 53, pp. 40–52.